Food Chemistry: X 18 (2023) 100735

Contents lists available at ScienceDirect

Food Chemistry: X

journal homepage: www.sciencedirect.com/journal/food-chemistry-x

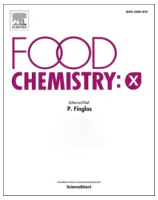

Preparation and characterization of soy protein isolate films by pretreatment with cysteine

Jialin Jiang [a], Linfan Shi [a,b], Zhongyang Ren [a,b], Wuyin Weng [a,b,*]

[a] College of Ocean Food and Biological Engineering, Jimei University, Xiamen 361021, China
[b] Fujian Provincial Engineering Technology Research Center of Marine Functional Food, Xiamen 361021, China

ARTICLE INFO

Keywords:
Soy protein isolate
Cysteine
Viscosity
Physicochemical properties
Edible films

ABSTRACT

The effect of cysteine concentration on the viscosity of soy protein isolate (SPI)-based film-forming solution (FFS) and physicochemical properties of SPI films was investigated. The apparent viscosity of FFS decreased after adding 1 mmol/L cysteine but did not change after adding 2–8 mmol/L cysteine. After treatment with 1 mmol/L cysteine, the film solubility decreased from 70.40% to 57.60%, but the other physical properties did not change. The water vapor permeability and contact angle of SPI films increased as cysteine concentration increased from 4 mmol/L to 8 mmol/L, whereas the film elongation at break decreased. Based on scanning electron microscopy and X-ray diffraction results, cysteine crystallization could be aggregated on the surface of SPI films treated with 4 or 8 mmol/L cysteine. In conclusion, pretreatment with approximately 2 mmol/L cysteine could reduce the viscosity of SPI-based FFS, but did not change the physicochemical properties of SPI films.

1. Introduction

The edible films prepared with natural biomaterials have gained global attention, because environmental pollution can be caused by the plastic waste of food packaging (Omar-Aziz et al., 2021). Soy protein isolate (SPI) has cheap and excellent film-forming capacity, and this material is expected to be industrialized as edible film material (Hu et al., 2022). The feasibility of industrial production with SPI films by using tape casting has been reported (Ortiz, de Moraes, Vicente, Laurindo, & Mauri, 2017). However, the long drying time limits the industrial production of tape casting for the preparation of edible films, because a large amount of water in the flowing film-forming solution (FFS) needs to evaporate during drying (Jeevahan et al., 2020). Therefore, improving the drying efficiency has become a key link in the industrial production of edible films by tape casting.

High solid concentration in the FFS induces shortened drying time and improves the drying rate. However, the viscosity of protein solution depends on the concentration and molecular weight of protein (Hong, Iwashita, & Shiraki, 2018; Xu, Han, Shi, Gao, & Li, 2020). Under high concentration, some proteins may not be dispersed and dissolved because of the high viscosity of protein dispersion solution (O'Flynn, Hogan, Daly, O'Mahony, & McCarthy, 2021). Thus, reducing the solution viscosity is a favorable approach to increase the solid concentration in the FFS, which can provide support for improving the drying rate. It was reported that the viscosity of protein solution was more effective to reduce by controlling the protein aggregation compared with the control of protein structure (Hong et al., 2018). Reducing agents can reduce the viscosity of protein solution (Qi, Li, Wang, & Sun, 2013), except via physical means such as heating and high-pressure homogenization (O'Flynn et al., 2021; Song, Zhou, Fu, Chen, & Wu, 2013). The viscosity of wheat flour solutions remarkably decreases after adding cysteine (Lambert & Kokini, 2001).

Cysteine can cleave the disulfide bonds of proteins because of the reducing properties of sulfhydryl groups (Xu & Yang, 2014). Cysteine can promote the formation of interchain disulfide bonds by the thiol/disulfide exchanges of protein molecules (Yang, Qian, Jiang, & Hou, 2021), thus improving the strength of whey-protein-based gels (Lavoisier, Vilgis, & Aguilera, 2019). The mechanical properties of SPI-gluten composite films were improved by 1% (*w/w*) cysteine at pH 7.0 because of the increased disulfide bonds (Were, Hettiarachchy, & Coleman, 1999). The elongation at break (EAB) of gelatin films increased with increasing cysteine concentration from 0.01% to 0.02%, but the tensile strength (TS) decreased with increasing cysteine concentration up to 0.04% (*w/w*) or more (Yu, Wang, & Yu, 2021). Although the physicochemical properties of protein films could be affected by cysteine, the effect of cysteine concentration on the

* Corresponding author at: College of Ocean Food and Biological Engineering, Jimei University, Xiamen 361021, China.
E-mail address: wwymail@jmu.edu.cn (W. Weng).

https://doi.org/10.1016/j.fochx.2023.100735
Received 28 January 2023; Received in revised form 29 May 2023; Accepted 1 June 2023
Available online 7 June 2023

properties of SPI films has not been reported.

The addition of cysteine can not only reduce the viscosity of SPI-based FFS, but also potentially improves the physicochemical properties of the SPI films. Therefore, the present study aimed to elucidate the effect of cysteine on the viscosity of SPI-based FFS and determine the physicochemical properties of resulting films. First, the correlation between the protein molecular weight and the viscosity of FFS based on SPI induced by cysteine was investigated. Then, the effect cysteine concentration on the physical properties of SPI films was clarified by analyzing the changes in protein interactions that maintain the protein film network structure. This study can reveal the influence mechanism of cysteine on SPI film formation from the perspective of reducing the viscosity of the FFS, providing the theoretical basis for the high-efficiency drying process of SPI films.

2. Materials and methods

2.1. Materials

SPI was obtained from Linyi Shansong Biological Products Co., Ltd. (Linyi, China). Cysteine and β-mercaptoethanol (β-ME) were obtained from Macklin Biochemical Co., Ltd. (Shanghai, China). Glycerol was obtained from Xilong Scientific Co., Ltd. (Shantou, China).

2.2. Preparation of film-forming solution and films.

SPI-based FFS was prepared by dissolving 6% (*w/v*) of SPI and 20% (*w/w*) of glycerol in distilled water containing cysteine concentrations of 0, 1, 2, 4, and 8 mmol/L. FFS was heated at 90 °C for 60 min in a water bath and defoamed before being cast in a rimmed silicon resin plate. Then, the plates with FFS were dried in a chamber (PSX-330H, Laifu Technology Co., Ltd., China) at a temperature of 25 ± 0.5 °C and humidity of 50% ± 5% for 24 h. The SPI films were peeled and equilibrated in the same chamber for 48 h before analysis.

2.3. Characterization of film-forming solution

2.3.1. Viscosity

The viscosity of FFS was measured using a DH-2 rheometer (TA Instruments, New Castle, USA) with a parallel plate (40 mm diameter and 1 mm gap) over a shear rate range of 1–1,000 s^{-1}.

2.3.2. Sodium dodecyl sulfate–polyacrylamide gel electrophoresis (SDS-PAGE)

SDS-PAGE was conducted as reported by Fang et al. (2021) by using 4% stacking gel and 10% resolving gel. After electrophoresis, the gel was stained with Coomassie Brilliant Blue R-250 dissolved in 5% methanol and 10% acetic acid (*v/v*), and then decolorized using a mixture of 30% methanol and 10% acetic acid (*v/v*). The electrophoretic samples of films were prepared by solubilizing SPI-based films in the solution containing 2% (*w/w*) SDS, 8 mol/L urea, and 20 mmol/L Tris-HCl (pH 8.8).

2.4. Characterization of SPI films

2.4.1. Mechanical properties

TS and EAB were measured using a texture analyzer (TA-XT Plus, Stable Micro System, UK), as reported by Hu et al. (2022). Before the analysis, the thickness of the film sample was recorded using a digital thickness gauge micrometer. The initial spacing for stretching was 30 mm, and the speed was set to 1 mm/s. The TS and EAB of the films were calculated according to formulas (1) and (2), respectively, as follows:

$$TS\ \left(MPa\right) = \frac{F_{\max}}{S} \tag{1}$$

$$EAB\ \left(\%\right) = \frac{E}{30} \times 100 \tag{2}$$

where F_{max} is the max force (N) required to pull the films, S is the area obtained by multiplying the thickness and width (mm^2), E is the length (mm) of the films at breaking, and 30 is the initial length (mm) of the films.

2.4.2. Water vapor permeability (WVP)

The measurement of WVP of films was performed as described by Hu et al. (2022). The plastic bottles with a neck diameter of 2.2 cm were filled with dried silicone (0% relative humidity) and sealed hermetically with films. Then, they were placed in a desiccator permeated with distilled water at a temperature of 30 °C (100% relative humidity). The weight of the bottles was recorded once an hour for nine times. The WVP was calculated as the previous report (Hu et al., 2021).

2.4.3. Optical properties

The L^*, a^*, and b^* values of films were determined using a colorimeter (WSC–S; Shanghai Precision & Scientific Instrument Co., China). The color parameters of films were measured on a whiteboard with the values of L^* (91.86), a^* (−0.88), and b^* (1.42).

The transparency of film sample was examined using a UV–visible spectrophotometer (UV-8000A; Shanghai Yuanxi Instrument Co., China) at the absorbance of 600 nm as described by Hu et al. (2022). The transparency values were calculated as the previous report (Hu et al., 2022).

2.4.4. Film solubility

The solubility of films was determined as described by Hu et al. (2021). The films were cut into identical squares (20 mm × 20 mm) and weighted before soaking in a bottle with 10 mL of distilled water. Then, the bottles were shaken in a water bath at 30 °C for 24 h. The solid–liquid mixture was filtered, and the solid was placed in the oven and dried at 105 °C for 24 h to a constant weight. The protein fraction of films dissolved in water was analyzed by SDS-PAGE. The solubility of SPI films in water was calculated as follows:

$$Solubility\ \ (\%) = \frac{m_0 - m_1}{m_0} \times 100 \tag{3}$$

where m_0 is the initial weight of films, and m_1 is the final weight of dried SP films.

2.4.5. Contact angle

The contact angle of the films was evaluated as described by Hu et al. (2021). The distilled water droplets were injected vertically on the film surface (10 mm × 40 mm) by using a contact angle analyzer (SDC-200, Shengding Precision Instrument Co., Ltd., China), and the photo was captured after 2 s. The software was used to calculate the angle between the water droplets and the surface of the SPI films.

2.4.6. Interaction analysis

In total, 20 mg SPI film powder was dissolved in 1 mL of different solutions, including S1 (0.6 mol/L NaCl), S2 (0.6 mol/L NaCl, 1.5 mol/L urea, S3 (0.6 mol/L NaCl, 8 mol/L urea), and S4 (0.6 mol/L NaCl, 8 mol/L urea, 0.5 mol/L β-ME), as described by Weng, Hamaguchi, Osako, & Tanaka. (2007). The centrifuge tubes containing the samples were gently shaken at 50 rpm for 24 h by using a shaker and centrifuged at 10,000 rpm for 30 min at room temperature The protein content was determined based in Lowry's method by using bovine serum albumin as the standard, and the total protein content of the films solubilized in 2 mol/L NaOH. The proportion of solubility of SPI films in S1, (S2–S1), (S3–S2), and (S4–S3) were used to characterize ionic bonding, hydrogen bonding, hydrophobic interactions, and disulfide bonding, respectively. The subunits distribution of SPI films dissolved in different denaturing

solutions were characterized by SDS-PAGE.

2.4.7. X-ray diffraction (XRD)

The XRD patterns of the SPI films were determined using an X-ray diffractometer (Ultima-IV, Rigaku, Japan) with an angular range of 5°–50° and Cu-Kα radiation (40 kV, 30 mA).

2.4.8. Scanning electron microscopy (SEM)

The microstructural analysis of the upper surfaces of the films was carried out using SEM (Phenom Pro, Phenom-World, NED) with an acceleration voltage of 5 kV at magnifications of 1,000 × and 10,000 ×.

2.5. Statistical analysis

The data were expressed as mean ± standard deviation. One-way analysis of variance (ANOVA) and Duncan multiple range test at $p < 0.05$ were used to evaluate the data statistically by using SPSS statistics 17.0 software (SPSS, Inc., Chicago, IL, USA).

3. Results

3.1. Characterization of film-forming solution

The effect of the shear rate on the apparent viscosity of FFS is shown in Fig. 1(a). The shear-thinning behavior of the FFS with the increase in shear rate indicates that FFS was essentially a pseudoplastic fluid. The apparent viscosity of the FFS at a shear rate of 1 s^{-1} decreased markedly from 41.60 mPa·s to 12.78 mPa·s after adding 1 mmol/L cysteine. A similar result was reported by Lambert & Kokini (2001), who suggested that the decrease in viscosity of wheat protein flour solutions is related to the cleavage of disulfide bonds between wheat proteins by cysteine. However, no significant difference was observed in the apparent viscosity of FFS after the concentration of cysteine was increased from 2 mmol/L to 8 mmol/L ($p > 0.05$). As shown in Fig. 1 (b), SPI mainly consists of α (72 kDa), α' (76 kDa), and β (53 kDa) from 7S, acidic subunits (As) and basic subunits (Bs) from 11S. The protein bands with molecular weights of 100–200 kDa disappeared when β-ME was added, implying that disulfide bonds were present in the SPI protein. In the non-reducing SDS-PAGE, the protein band intensity with molecular weights of 100–200 kDa gradually disappeared with increasing cysteine concentration, whereas the band intensity of α and α' subunits increased, suggesting that the protein with weight of 100–200 kDa was formed by α and α' subunits via disulfide bonds. In comparison with the non-reducing SDS-PAGE, the band intensity of the As and Bs subunits in the reducing SDS-PAGE increased. However, no obvious difference was observed in the band intensity of α and α' subunits with different cysteine concentrations in the reducing SDS-PAGE. The results in Fig. 1 suggest that the disulfide bonds that link the α and α' subunits could be cleaved by cysteine, resulting in a decrease in SPI-based FFS viscosity.

3.2. Characterization of soy protein films

3.2.1. Mechanical properties

The TS and EAB of SPI films were 7.75 MPa and 122.51%, respectively (Table 1), and these values were close to those of the reported SPI films (TS = 6.3 MPa, EAB = 177.97%; Li et al., 2021). No obvious difference was observed in the effect of cysteine concentration on the TS of SPI films (Table 1). However, the EAB of SPI films significantly decreased after adding at least 4 mmol/L cysteine ($p < 0.05$).

3.2.2. WVP

The effect of cysteine concentration on the WVP of SPI films is shown in Table 1. The WVP of SPI films was 0.86 × 10^{-10} g·m^{-1}·s^{-1}·pa^{-1}, which was lower than that of the reported SPI films (1.33 × 10^{-10} g·m^{-1}·s^{-1}·pa^{-1}; Han & Wang, 2016). The WVP of SPI films was not significantly different when the concentration of the cysteine added was not higher than 4 mmol/L ($p > 0.05$), but WVP increased and reached 1.19 × 10^{-10} g·m^{-1}·s^{-1}·pa^{-1} after the addition of 8 mmol/L cysteine.

3.2.3. Optical properties

The optical properties of the SPI films with different cysteine concentrations were characterized in terms of color and transparency values (Table 2). The color parameters, namely, the L^*, a^*, and b^* values of SPI films were 81.55, –2.54, and 17.34, respectively. There was no significant difference in the color parameters of the films after adding 1 or 2 mmol/L cysteine. When the cysteine concentration was further increased, the L^* value decreased, whereas the a^* value increased significantly ($p < 0.05$).

Table 1
Effect of cysteine concentration on the mechanical properties and WVP of SPI films.

Cysteine (mmol/L)	TS (MPa)	EAB (%)	WVP (×10^{-10} g·m^{-1}·s^{-1}·pa^{-1})
0	7.75 ± 0.31[a]	122.51 ± 19.99[a]	0.86 ± 0.13[b]
1	7.09 ± 0.52[a]	103.66 ± 33.56[a]	0.92 ± 0.10[b]
2	7.64 ± 0.49[a]	127.28 ± 18.72[a]	0.91 ± 0.10[b]
4	7.88 ± 0.64[a]	81.44 ± 26.38[b]	0.94 ± 0.12[b]
8	7.86 ± 0.34[a]	55.86 ± 19.77[c]	1.19 ± 0.06[a]

Data are expressed as mean ± standard deviation.
Values with different lower-case letters in the same column indicate significant differences at $p < 0.05$.

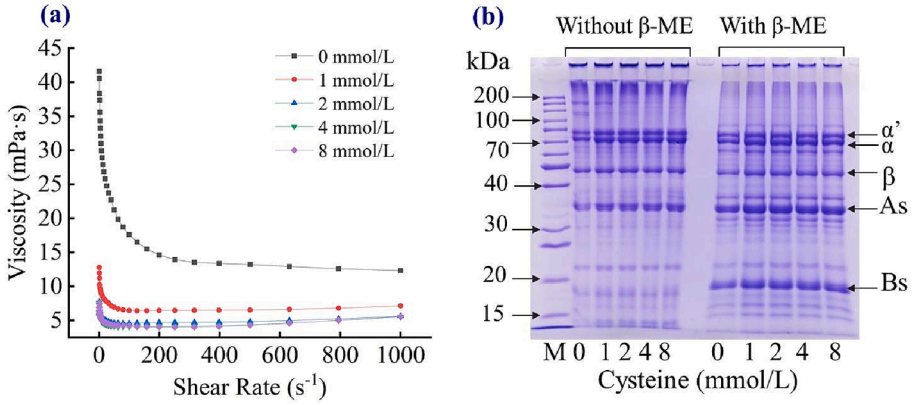

Fig. 1. Apparent viscosity versus shear rate (a) and SDS-PAGE patterns (b) of FFS at different cysteine concentrations.

Table 2
Effect of cysteine concentration on the optical properties and transparency of SPI films.

Cysteine (mmol/L)	Color			Transparency value
	L^*	a^*	b^*	
0	81.55 ± 0.30^a	−2.54 ± 0.06^d	17.34 ± 0.49^a	0.61 ± 0.11^c
1	81.52 ± 0.19^a	−2.28 ± 0.06^c	17.28 ± 0.29^a	0.61 ± 0.18^c
2	81.05 ± 0.39^b	−2.29 ± 0.06^c	17.40 ± 0.51^a	0.95 ± 0.17^c
4	80.87 ± 0.27^b	−2.02 ± 0.04^b	17.88 ± 0.51^a	1.75 ± 0.12^b
8	79.89 ± 0.31^c	−1.72 ± 0.14^a	17.72 ± 0.41^a	2.66 ± 0.84^a

Data are expressed as mean ± standard deviation.
Values with different lower-case letters in the same column indicate significant differences at $p < 0.05$.

The transparency value of the pure SPI films was 0.61 (Table 2), which was close to that of SPI films treated with 1 or 2 mmol/L cysteine. However, the transparency value of SPI films increased remarkably ($p < 0.05$) after FFS was treated with 4 or 8 mmol/L cysteine. Therefore, low concentrations of cysteine insufficiently altered the transparency of SPI films.

3.2.4. Film soluble characteristics

The solubility of the SPI films treated with cysteine is presented in Fig. 2(a). The solubility of SPI films was 70.40%, which decreased significantly ($p < 0.05$) with the increase in cysteine concentration from 0 to 4 mmol/L. However, the solubility of SPI films changed insignificantly when the cysteine concentration was further increased ($p > 0.05$). The protein in the films dissolved in water was analyzed by SDS-PAGE (Fig. 2b). In the non-reducing SDS-PAGE, the high molecular weight fractions (HMWF) at the top of the polyacrylamide gel gradually decreased with the increase in cysteine concentration, whereas the other protein patterns did not change obviously (Fig. 2b), indicating that water-insoluble aggregates could be formed from HMWF induced by cysteine. In comparison with the films dissolved in denaturing solution (Fig. S1), the band intensities of β and Bs subunits were weaker in the films dissolved in water, whereas the other band intensities were similar (Fig. 2b), suggesting that the β and Bs subunits played an important role in the water resistance of SPI films.

3.2.5. Contact angle

The contact angle can represent the surface polarity of protein films, and this parameter can be used to select the application range (Rodríguez-Félix et al., 2022). As shown in Table 3, the contact angles of the upper and lower surfaces from the SPI films were 84.72° and 85.61°, respectively, suggesting that the surface of the prepared SPI films possessed hydrophilic characteristics. As cysteine concentration was increased to 4 mmol/L, the contact angles of both the upper and lower surfaces of SPI films decreased slightly. However, the film contact angle at the upper and lower surfaces exceeded 90° when the cysteine concentration was 8 mmol/L.

Table 3
Effect of cysteine concentration on the contact angle of SPI films.

Cysteine (mmol/L)	Contact angle (°)	
	Upper surface	Lower surface
0	84.72 ± 4.08^b	85.61 ± 4.91^b
1	80.72 ± 5.20^{bc}	83.87 ± 6.08^b
2	78.37 ± 4.17^c	82.79 ± 1.92^b
4	77.35 ± 4.33^c	80.66 ± 4.16^b
8	91.25 ± 2.70^a	92.90 ± 2.77^a

Data are expressed as mean ± standard deviation.
Values with different lower-case letters in the same column indicate significant differences at $p < 0.05$.

3.2.6. Interaction analysis

The SDS-PAGE patterns of SPI films dissolved in different denaturing solutions are presented in Fig. 3(a). In the protein patterns of the films dissolved in S1, the α, α', and As subunits were observed, and their band intensity increased slightly with the increase in cysteine concentration. Similar subunit bands were also observed in the SDS-PAGE patterns of films dissolved in S2–S1. Therefore, the α, α', and As subunits are involved in the SPI film formation through ionic and hydrogen bonds. However, the band intensity of HMWF1 dissolved in S1 and S2–S1 could not enter the separating gel and gradually decreased with increasing cysteine concentration, indicating that cysteine could prevent HMWF1 from participating in ionic and hydrogen bond formation. In the protein patterns of films dissolved in S3–S2, the HMWF1, HMWF2, and 7S subunits were observed, indicating that the HMWF and 7S subunits were involved in hydrophobic interactions during film formation. Notably, the 7S and 11S subunits were observed in the SDS-PAGE patterns of films dissolved in S4–S3, suggesting that all SPI subunits could be involved in the film formation through disulfide bonds. Based on SDS-PAGE, the protein fractions involved in the hydrophobic interactions and disulfide bonds of SPI films were not affected by the cysteine concentration.

The effect of cysteine concentration on the interaction between proteins in SPI films is shown in Fig. 3(b). The percentages of ionic bonds, hydrogen bonds, hydrophobic interactions, and disulfide bonds in the SPI films were 20.82%, 16.57%, 25.07%, and 27.66%, respectively. When FFS was treated with 1 mmol/L cysteine, the percentage of hydrophobic interactions in the formed films increased to 37.71%, whereas the percentage of disulfide bonds decreased to 14.80%, suggesting that the interaction between the exposed hydrophobic groups

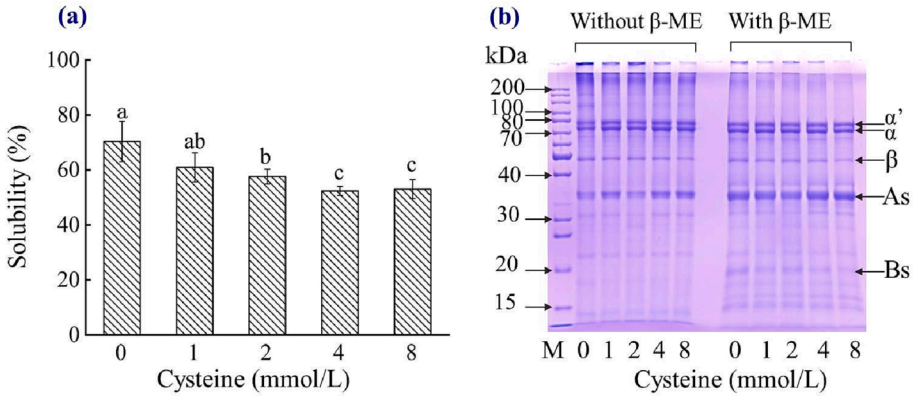

Fig. 2. Solubility of SPI films dissolved in water (a) and SDS-PAGE patterns of soluble protein fraction (b).

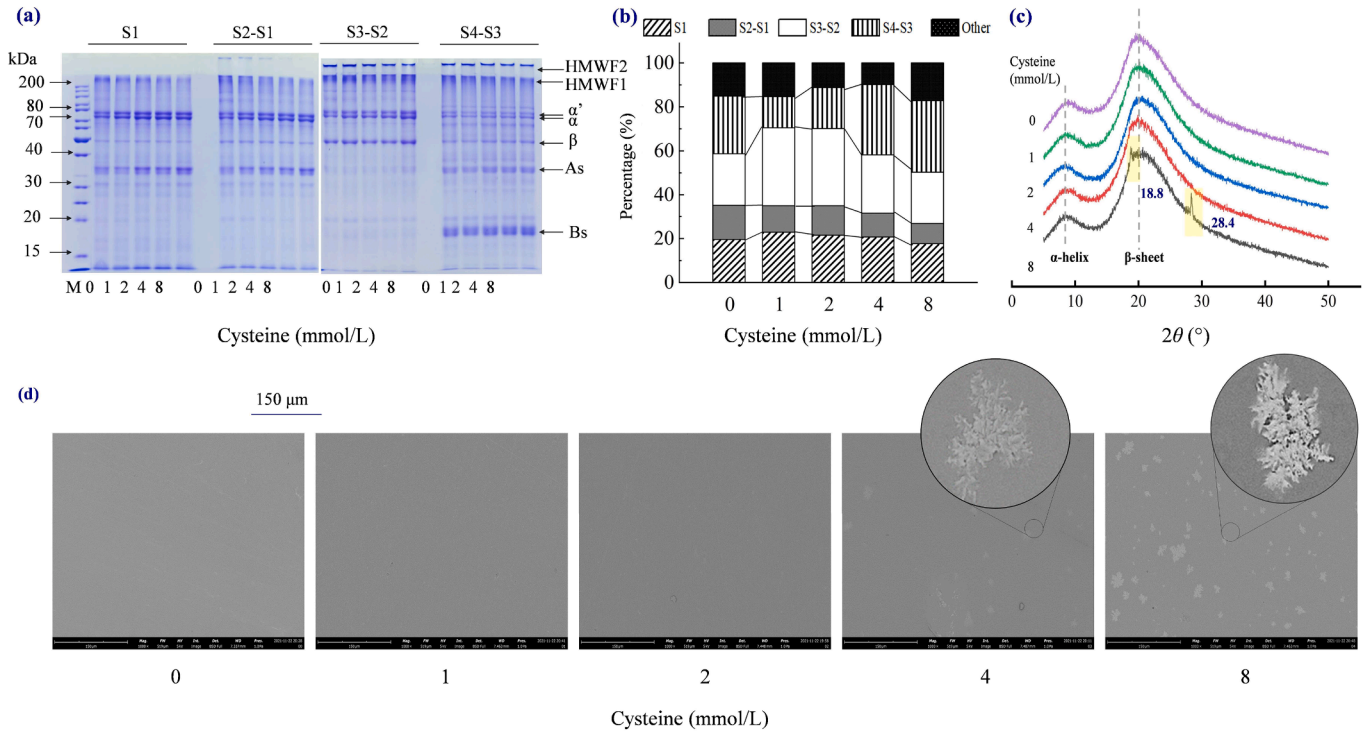

Fig. 3. Effect of cysteine concentration on the SDS-PAGE patterns of SPI films dissolved in denaturing solutions (a), percentage of chemical bonds (b), XRD patterns (c), and XRD patterns (d) of SPI films.

was enhanced after the disulfide bonds in SPI were cleaved by cysteine. The disulfide bond in α-lactalbumin protein could be cleaved by 0.35–1.4 mmol/L cysteine, thus increasing the number of exposed hydrophobic groups (Nielsen, Lund, Davies, Nielsen, & Nielsen, 2018); however, the formation of disulfide bonds in the cold-extruded whey protein could be promoted by the addition of 15 mmol/L cysteine, because cysteine could induce the thiol/disulfide exchanges of protein (Yang et al., 2021). A similar phenomenon was observed in the SPI films treated with 0–4 mmol/L cysteine, but the results of the present study demonstrate that 8 mmol/L cysteine could promote the formation of non-disulfide covalent bonds in the SPI films.

3.2.7. *XRD analysis*

The XRD patterns of SPI films are shown in Fig. 3(c). Two diffraction peaks at 2θ values of approximately 8.85° and 19.56° were found in the SPI films, and these values correspond to the α-helix and β-sheet crystalline structures of amorphous globulins (Li et al., 2021; Hu et al., 2022). No obvious changes were observed in the intensity and position of diffraction peaks when SPI films were prepared after treatment with 4 mmol/L cysteine or less. When the cysteine concentration reached 8 mmol/L, two new diffraction peaks at 2θ values of approximately 18.8° and 28.4° appeared in the SPI films, and these values could be attributed to cysteine (Su et al., 2022). Therefore, the excessive amount of cysteine easily formed crystals in the prepared SPI films.

3.2.8. *SEM*

The microstructure of SPI films is shown in Fig. 3(d). The surface of SPI films was flat, homogeneous, and smooth. No obvious changes were observed on the surface of SPI films with the addition of 1 or 2 mmol/L cysteine. When at least 4 mmol/L cysteine was added, some aggregates appeared on the film surface (Fig. 3d). Especially, the surface of SPI films with 8 mmol/L cysteine showed snowflake-like aggregates, which could be attributed to the excessive amount of cysteine detected by XRD (Fig. 3c). Therefore, high concentrations of cysteine could accumulate during film drying and form particles on the film surface.

4. Discussion

The low viscosity of protein based FFS can increase SPI solids, which is conductive to improving the drying rate of protein films. In general, the viscosity of proteins could be enhanced by the combined effect of molecular interactions and molecular weight (Averina, Konnerth, D'Amico, & van Herwijnen, 2021). The viscosity of SPI solution decreased remarkably after adding sodium bisulfite possibly because of the rapture of disulfide bonds (Qi et al., 2013), while the whey protein isolate-based films with sodium sulfite had a poor EAB (Schmid, Prinz, Stäbler, & Sängerlaub, 2017). However, the effect of sodium sulfite on the viscosity of protein-based FFS and physicochemical properties of protein films has not been reported. The viscosity of SPI solution decreased by 87.7% after adding 0.4% (w/w) bromelain due to the breakage of the peptide bonds (Xu et al., 2020), but the effect of bromelain on the physicochemical properties of SPI films has not been evaluated. In present study, the viscosity of the SPI-based FFS decreased by 69.3% after adding 1 mmol/L cysteine, but the TS and EAB of the formed SPI films were not significantly affected (Table 1). Therefore, the breakage of disulfide bonds only reduces the viscosity of SPI-based FFS and does not affect the film-forming ability of SPI. When the SPI was added at least 4 mmol/L cysteine, the viscosity of the FFS could not be further reduced while the EAB of films decreased significantly ($p < 0.05$), possibly because the cysteine crystals destroyed the film's extensibility (Table 1, Figs. 1a, 3c, and 3d).

The mechanical properties of protein-based films are determined based on the protein structure, intermolecular interactions, and film's microstructure (Omar-Aziz et al., 2021; Weng & Zheng, 2015; Xu et al., 2021). In the present study, the subunits in 7S participate in the formation of SPI film network structure through ionic bonds, hydrogen bonds, hydrophobic interactions, and disulfide bonds, whereas the subunits in 11S are mainly involved through disulfide bonds. The disulfide bonds among the SPI protein molecules were broken upon the addition of 1 mmol/L cysteine, thus enhancing the hydrophobic interactions in the formed SPI films. However, the ratio of disulfide bonds in SPI films increased slightly with increasing cysteine concentration.

This finding was obtained possibly because cysteine can initiate the thiol/disulfide exchange reactions of protein molecules and promote protein polymerization (Yang et al., 2021). The toughness of sunflower protein films decreased when the added tannins exceeded the maximum amount bound to the protein network (Orliac, Rouilly, Silvestre, & Rigal, 2002). The addition of cysteine led to the decrease in EAB of gliadin films because of the formation of disulfide bonds between protein molecules (Hernandez-Munoz, Kanavouras, Villalobos, & Chiralt, 2004). In the present study, cysteine disrupted the network structure of SPI films (Fig. 3d), thus decreasing the flexibility and WVP (Table 1). Moreover, a significant increase in the transparency values of SPI films was observed with increasing cysteine concentrations (Table 2; $p < 0.05$), suggesting that the crystals formed from the excessive cysteine affected film's light scattering. Similarly, the transparency values of the composite films based on psyllium seed gum (PSG) and whey protein isolate were increased after adding PSG (Zhang, Zhao, Li, Zhu, Fang, & Shi, 2020). In conclusion, the physicochemical properties of SPI films are influenced by the protein interactions and structure network induced by the added cysteine.

The water solubility of protein-based edible films is influenced by the protein interactions of maintaining network structural integrity, which may also be a measure of film's water resistance (Fakhouri et al., 2018; Luo et al., 2022). The water resistance of protein-based films could be improved with the formed network polymers induced by the hydrophobic interactions (Jiang, Xiong, Newman, & Rentfrow, 2012), disulfide bonds (Ciannamea, Stefani, & Ruseckaite, 2014), and covalent crosslinkings (Liu et al., 2017). In the present study, the water solubility of SPI films significantly decreased after 1 or 2 mmol/L cysteine was added ($p < 0.05$), possibly because hydrophobic interactions played a key role in the film's water resistance. When the concentration of added cysteine reached 4 mmol/L, the decrease in the water solubility of SPI films might be related to the increase in disulfide bond proportion. When the concentration of added cysteine was further increased to 8 mmol/L, no significant changes were observed in the water solubility of SPI films and the proportion of disulfide bonds ($p > 0.05$) despite the increase in the proportion of covalent bonds. Therefore, the water resistance of cysteine-induced SPI films was mainly affected by hydrophobic interactions and disulfide bonds. Moreover, the β and Bs subunits might play an important role in the water resistance of SPI films (Figs. 2 and S1). The film's contact angle decreased slightly as the cysteine concentration gradually increased to 4 mmol/L (Table 3), possibly because the exposed hydrophobic groups induced by cysteine aggregated through hydrophobic interactions (Fig. 3b). A similar phenomenon was reported by Zhang et al. (2022), who found that the exposed hydrophobic groups by denaturation were involved in hydrophobic interactions, resulting in the decreased surface hydrophobicity of pea proteins. However, the contact angle of the SPI films with 8 mmol/L cysteine was higher than that of other films (Table 3), possibly because of the formation of non-disulfide covalent bonds (Fig. 3b).

5. Conclusion

This study revealed the influence of cysteine concentration on the viscosity of SPI-based FFS and the physicochemical properties of the films. The apparent viscosity of FFS was reduced by cysteine, because the disulfide bonds in the α and α' subunits of the SPI were cleaved. However, the mechanical properties and optical properties of the SPI films were unaffected after FFS was treated with 2 mmol/L cysteine or less, because the hydrophobic interactions increased from cysteine-induced exposed hydrophobic groups. The EAB of SPI films increased as the cysteine concentrations increased to 4 mmol/L or more because of the formation of crystals on the SPI film's surface after adding excessive cysteine. Overall, the viscosity of SPI-based FFS can be reduced by pretreatment with approximately 2 mmol/L cysteine concentration, which can provide a new way to increase drying efficiency.

CRediT authorship contribution statement

Jialin Jiang: Methodology, Data curation, Writing – original draft. **Linfan Shi:** Writing – review & editing. **Zhongyang Ren:** Writing – review & editing. **Wuyin Weng:** Conceptualization, Writing – review & editing.

Declaration of Competing Interest

The authors declare that they have no known competing financial interests or personal relationships that could have appeared to influence the work reported in this paper.

Data availability

The authors do not have permission to share data.

Acknowledgements

This work is sponsored by National Natural Science Foundation of China (32272266), National Key R&D Program of China (2021YFD2100204), and Fujian Science and Technology Project (2021N5013).

Appendix A. Supplementary data

Supplementary data to this article can be found online at https://doi.org/10.1016/j.fochx.2023.100735.

References

Averina, E., Konnerth, J., D'Amico, S., & van Herwijnen, H. W. (2021). Protein adhesives: Alkaline hydrolysis of different crop proteins as modification for improved wood bonding performance. *Industrial Crops and Products, 161*, Article 113187.

Ciannamea, E. M., Stefani, P. M., & Ruseckaite, R. A. (2014). Physical and mechanical properties of compression molded and solution casting soybean protein concentrate based films. *Food Hydrocolloids, 38*, 193–204.

Fakhouri, F. M., Martelli, S. M., Caon, T., Velasco, J. I., Buontempo, R. C., Bilck, A. P., et al. (2018). The effect of fatty acids on the physicochemical properties of edible films composed of gelatin and gluten proteins. *LWT, 87*, 293–300.

Fang, Q., Shi, L., Ren, Z., Hao, G., Chen, J., & Weng, W. (2021). Effects of emulsified lard and TGase on gel properties of threadfin bream (*Nemipterus virgatus*) surimi. *LWT, 146*, Article 111513.

Han, Y., & Wang, L. (2016). Improved water barrier and mechanical properties of soy protein isolate films by incorporation of SiO 2 nanoparticles. *RSC Advances, 6*(113), 112317–112324.

Hernandez-Munoz, P., Kanavouras, A., Villalobos, R., & Chiralt, A. (2004). Characterization of biodegradable films obtained from cysteine-mediated polymerized gliadins. *Journal of Agricultural and Food Chemistry, 52*(26), 7897–7904.

Hong, T., Iwashita, K., & Shiraki, K. (2018). Viscosity control of protein solution by small solutes: A review. *Current Protein and Peptide Science, 19*(8), 746–758.

Hu, Y., Shi, L., Ren, Z., Hao, G., Chen, J., & Weng, W. (2021). Characterization of emulsion films prepared from soy protein isolate at different preheating temperatures. *Journal of Food Engineering, 309*, Article 110697.

Hu, Y., Yang, S., Zhang, Y., Shi, L., Ren, Z., Hao, G., et al. (2022). Effects of microfluidization cycles on physicochemical properties of soy protein isolate-soy oil emulsion films. *Food Hydrocolloids, 130*, Article 107684.

Jeevahan, J. J., Chandrasekaran, M., Venkatesan, S. P., Sriram, V., Joseph, G. B., Mageshwaran, G., et al. (2020). Scaling up difficulties and commercial aspects of edible films for food packaging: A review. *Trends in Food Science & Technology, 100*, 210–222.

Jiang, J., Xiong, Y. L., Newman, M. C., & Rentfrow, G. K. (2012). Structure-modifying alkaline and acidic pH-shifting processes promote film formation of soy proteins. *Food Chemistry, 132*(4), 1944–1950.

Lambert, I. A., & Kokini, J. L. (2001). Effect of L-cysteine on the rheological properties of wheat flour. *Cereal Chemistry, 78*(3), 226–230.

Lavoisier, A., Vilgis, T. A., & Aguilera, J. M. (2019). Effect of cysteine addition and heat treatment on the properties and microstructure of a calcium-induced whey protein cold-set gel. *Current Research in Food Science, 1*, 31–42.

Li, T., Xia, N., Xu, L., Zhang, H., Zhang, H. J., Chi, Y. J., et al. (2021). Preparation, characterization and application of SPI-based blend film with antioxidant activity. *Food Packaging and Shelf Life, 27*, Article 100614.

Liu, F., Chiou, B. S., Avena-Bustillos, R. J., Zhang, Y. Z., Li, Y., McHugh, T. H., et al. (2017). Study of combined effects of glycerol and transglutaminase on properties of gelatin films. *Food Hydrocolloids, 65*, 1–9.

Luo, Q., Hossen, M. A., Zeng, Y., Dai, J., Li, S., Qin, W., et al. (2022). Gelatin-based composite films and their application in food packaging: A review. *Journal of Food Engineering, 313*, Article 110762.

Nielsen, L. R., Lund, M. N., Davies, M. J., Nielsen, J. H., & Nielsen, S. B. (2018). Effect of free cysteine on the denaturation and aggregation of holo α-lactalbumin. *International Dairy Journal, 79*, 52–61.

O'Flynn, T. D., Hogan, S. A., Daly, D. F., O'Mahony, J. A., & McCarthy, N. A. (2021). Rheological and solubility properties of soy protein isolate. *Molecules, 26*(10), 3015.

Omar-Aziz, M., Gharaghani, M., Hosseini, S. S., Khodaiyan, F., Mousavi, M., Askari, G., et al. (2021). Effect of octenylsuccination of pullulan on mechanical and barrier properties of pullulan-chickpea protein isolate composite film. *Food Hydrocolloids, 121*, Article 107047.

Orliac, O., Rouilly, A., Silvestre, F., & Rigal, L. (2002). Effects of additives on the mechanical properties, hydrophobicity and water uptake of thermo-moulded films produced from sunflower protein isolate. *Polymer, 43*(20), 5417–5425.

Ortiz, C. M., de Moraes, J. O., Vicente, A. R., Laurindo, J. B., & Mauri, A. N. (2017). Scale-up of the production of soy (*Glycine max L.*) protein films using tape casting: Formulation of film-forming suspension and drying conditions. *Food Hydrocolloids, 66*, 110–117.

Qi, G., Li, N., Wang, D., & Sun, X. S. (2013). Adhesion and physicochemical properties of soy protein modified by sodium bisulfite. *Journal of the American Oil Chemists' Society, 90*(12), 1917–1926.

Rodríguez-Félix, F., Corte-Tarazón, J. A., Rochín-Wong, S., Fernández-Quiroz, J. D., Garzón-García, A. M., Santos-Sauceda, I., et al. (2022). Physicochemical, structural, mechanical and antioxidant properties of zein films incorporated with no-ultrafiltered and ultrafiltered betalains extract from the beetroot (*Beta vulgaris*) bagasse with potential application as active food packaging. *Journal of Food Engineering, 334*, Article 111153.

Schmid, M., Prinz, T. K., Stäbler, A., & Sängerlaub, S. (2017). Effect of sodium sulfite, sodium dodecyl sulfate, and urea on the molecular interactions and properties of whey protein isolate-based films. *Frontiers in Chemistry, 4*, 49.

Song, X., Zhou, C., Fu, F., Chen, Z., & Wu, Q. (2013). Effect of high-pressure homogenization on particle size and film properties of soy protein isolate. *Industrial Crops and Products, 43*, 538–544.

Su, Y., Hessou, E. P., Colombo, E., Belletti, G., Moussadik, A., Lucas, I. T., et al. (2022). Crystalline structures of l-cysteine and l-cystine: A combined theoretical and experimental characterization. *Amino Acids, 54*(8), 1123–1133.

Weng, W., Hamaguchi, P. Y., Osako, K., & Tanaka, M. (2007). Effect of endogenous acid proteinases on the properties of edible films prepared from Alaska pollack surimi. *Food Chemistry, 105*(3), 996–1002.

Weng, W., & Zheng, H. (2015). Effect of transglutaminase on properties of tilapia scale gelatin films incorporated with soy protein isolate. *Food Chemistry, 169*, 255–260.

Were, L., Hettiarachchy, N. S., & Coleman, M. (1999). Properties of cysteine-added soy protein-wheat gluten films. *Journal of Food Science, 64*(3), 514–518.

Xu, Y., Han, Y., Shi, S. Q., Gao, Q., & Li, J. (2020). Preparation of a moderate viscosity, high performance and adequately-stabilized soy protein-based adhesive via recombination of protein molecules. *Journal of Cleaner Production, 255*, Article 120303.

Xu, Y. P., Wang, Y., Zhang, T., Mu, G. Q., Jiang, S. J., Zhu, X. M., et al. (2021). Evaluation of the properties of whey protein films with modifications. *Journal of Food Science, 86*(3), 923–931.

Xu, H., & Yang, Y. (2014). Controlled de-cross-linking and disentanglement of feather keratin for fiber preparation via a novel process. *ACS Sustainable Chemistry & Engineering, 2*(6), 1404–1410.

Yang, N., Qian, S., Jiang, Z., & Hou, J. (2021). Cysteine inducing formation and reshuffling of disulfide bonds in cold-extruded whey protein molecules: From structural and functional characteristics to cytotoxicity. *Food Chemistry, 360*, Article 130121.

Yu, H., Wang, B., & Yu, P. (2021). The Influence of Cysteine on the Performances of Gelatin Film. *In IOP Conference Series: Earth and Environmental Science* (Vol. 697, No. 1, p. 012011). IOP Publishing, England and Wales.

Zhang, J., Liu, Q., Chen, Q., Sun, F., Liu, H., & Kong, B. (2022). Synergistic modification of pea protein structure using high-intensity ultrasound and pH-shifting technology to improve solubility and emulsification. *Ultrasonics Sonochemistry, 88*, Article 106099.

Zhang, X., Zhao, Y., Li, Y., Zhu, L., Fang, Z., & Shi, Q. (2020). Physicochemical, mechanical and structural properties of composite edible films based on whey protein isolate/psyllium seed gum. *International Journal of Biological Macromolecules, 153*, 892–901.